

# Numerical simulation of gas production in different layers in Shenhu area, South China Sea

Changwen Xiao<sup>1,2,3</sup>, Xiaosen Li<sup>1,2,3\*</sup>, Gang Li<sup>2\*</sup>, Yang Yu<sup>1,3\*</sup>, Jianxing Yu<sup>1,3</sup>

1 Key Laboratory of Hydraulic Engineering Simulation and Safety, Tianjin University, Tianjin, 300072, China

2 Key Laboratory of Gas Hydrate, Guangzhou Institute of Energy Conversion, Chinese Academy of Sciences, Guangzhou 510640, China

3 Tianjin Key Laboratory of Port and Ocean Engineering, Tianjin University, Tianjin, 300072, China

## ABSTRACT

The hydrate reservoir in Shenhu area is a complex, multilayered system and the production strategy of the target layer is the key to long-term efficient exploitation. According to available geological data, we used numerical simulation to analyze three cases of gas production in different layers by using the depressurization method with vertical wells. The production behaviors and evolutions of pressure, temperature, gas, and hydrate saturation were analyzed. The results showed that the depressurization rate was limited by the low permeability. For 10 years of production, the production case in the free-gas layer could obtain the largest cumulative gas production, and hydrate dissociation could obtain stable gas production.

**Keywords:** hydrate, Shenhu area, gas production, different layers, low-permeability

## NONMENCLATURE

### Abbreviations

CGS	China Geological Survey
NGH	Natural gas hydrate
T+H	TOUGH + HYDRATE

### Symbols

$P$	Pressure (MPa)
$R_{GW}$	gas-to-water ratio (-)
$S_A$	Water saturation (-)
$S_G$	Gas saturation (-)
$S_H$	Hydrate saturation (-)
$T$	Temperature (°C)
$V_{dg}$	Daily gas production (m <sup>3</sup> /day)
$V_{dw}$	Daily water production (m <sup>3</sup> /day)
$V_G$	Cumulative gas production (m <sup>3</sup> )
$V_W$	Cumulative water production (m <sup>3</sup> )
$k$	Intrinsic permeability (mD)
$\phi$	Porosity (-)

## 1. INTRODUCTION

Natural gas hydrate (NGH), also known as combustible-ice, is a crystalline compound with water and methane molecules under high pressure and low

temperature conditions [1, 2]. The natural gas stored in gas hydrate reservoirs is about  $2 \times 10^{16}$  m<sup>3</sup>, far exceeding the total organic carbon of traditional fossil energy such as oil and coal [3]. Since 2002, Canada, United States and Japan have carried out hydrate production tests in the Mallik site, Ignik Sikumi Field and Nankai Trough, by using thermal stimulation, CO<sub>2</sub>/N<sub>2</sub> replacement and depressurization, respectively [4-8]. These production tests showed that the depressurization is considered to be the most efficient and economical method for gas recovery from hydrate reservoirs.

Many studies reported that South China Sea contained large amounts of NGH resources, and its northern continental slope had favorable conditions for the hydrate formation and accumulation [9, 10]. In 2017 and 2020, China Geological Survey (CGS) successfully carried out two short-term NGH production test in Shenhu area, South China Sea, by using depressurization [11, 12]. The first production test had achieved an accumulative gas production of  $30.90 \times 10^4$  m<sup>3</sup> for 60 days. The second production test located in the same area, had finished an accumulative gas production of  $86.14 \times 10^4$  m<sup>3</sup> for 30 days. However, the gas production efficiency was still far from the commercial production of hydrate reservoirs. The main reason was that most offshore NGH reservoirs occurred in high water content and non-diagenetic sediments with a low permeability of several millidarcy, which had low hydrate dissociation efficiency. The dissociation of hydrate required the absorption of a large amount of heat, and the external heat supply was very limited. The utilization of the free gas in the reservoirs was the key to improve gas production efficiency in the hydrate reservoirs.

In order to achieve the commercial exploitation of NGH reservoirs, the important target is to find hydrate-bearing reservoirs of high permeability and high gas/hydrate saturation [12]. In large-scale high hydrate saturation reservoirs, natural gas mainly originates from

the migration of  $t^1$  hermogetic cracking gas in the hydrocarbon-generating window of deep sediments. These hydrate reservoirs are complex multilayer systems that accompanies by the enrichment of free gas in the underlying zone. There are mainly three types of multilayers [13]. Class 1 is composed of a hydrate-bearing layer, and an underlying two-phase fluid layer with mobile gas and water. Class 2 accumulations comprise two zones: a hydrate-bearing layer, and an underlying mobile water layer with no free gas. Class 3 contains only one hydrate-bearing layer. Another Class 4 is a low saturation and disperse hydrate reservoir without economical values. The hydrate reservoirs are mainly Class 1, with an underlying layer rich of free gas. Though the hydrate-bearing layer has huge natural gas resources, the existence of free gas has an important influence on gas production from hydrate reservoirs [13]. At present, there is a lack of theoretical understanding of the influence mechanism on the gas production efficiency of different layers. Generally, the production target in different layers would have different production behaviors and reservoir performances. Hence, the design of production strategies in different layers can effectively improve gas production efficiency.

In order to understand the production mechanism in different layers, we used TOUGH+HYDRATE simulation to analyze the gas production in different layers based on the available geological data of Shenhu area, South China Sea. The depressurization with flexible vertical wells was chose to be the production method. The production behaviors and reservoir performances was analyzed in detail. It would provide theoretical support and guidance for the selection of the target area for the exploitation of offshore hydrate reservoirs.

## 2. GEOLOGICAL BACKGROUND AND SIMULATION MODEL

### 2.1 Geological background

As shown in Fig. 1, the target area, marked as SHSC-4, was located at the site W17 in Shenhu area, part of Baiyun Sag of Pearl River Mouth Basin, South China Sea, where the first NGH production test was conducted in 2017. The water depth of the target area was 1266 m, and the seafloor temperature was in range of 3~5 °C. The hydrate deposit at site W17 were north-south trending, with an area of about 6.42 km<sup>2</sup> and an average thickness of about 57 m. The hydrate deposit had suitable thermodynamic conditions for the hydrate formation and accumulation. According to the analysis of the core samples, the sediment of the hydrate deposit was a low-

permeability reservoir with fine-grained clayey silt of an average particle size of about 12 μm, and the main component was clay [14]. The hydrate deposit at site W17 was similar to Class 1, which had two hydrate-bearing layers (e.g. a two-phase hydrate-bearing layer with fissures being filled with water and hydrate, and a three-phase mixing layer with mobile gas, water and hydrate), and an underlying two-phase fluid layer with mobile gas and water.

As reported [11], the hydrate deposit of the target area were including: Hydrate layer I (HYDRA), which is -1530~-1495 m below sea level, and its permeability  $k$  is 2.9 mD, the porosity  $\phi$  is 35%, and the water and hydrate saturations in the pores are  $S_A = 66\%$  and  $S_H = 34\%$ , respectively. Hydrate layer II (HYDRB), located at -1545~-1530 m below sea level, with a permeability  $k$  of 1.5 mD, a porosity  $\phi$  of 33%,  $S_H = 31\%$ ,  $S_G = 7.8\%$  and  $S_A = 61.2\%$  respectively. Free gas layer (MUDDY), located at -1572~-1545 m below sea level, with a permeability  $k$  of 7.4 mD, a porosity  $\phi$  of 32%,  $S_G = 7.8\%$  and  $S_A = 92.2\%$  respectively.

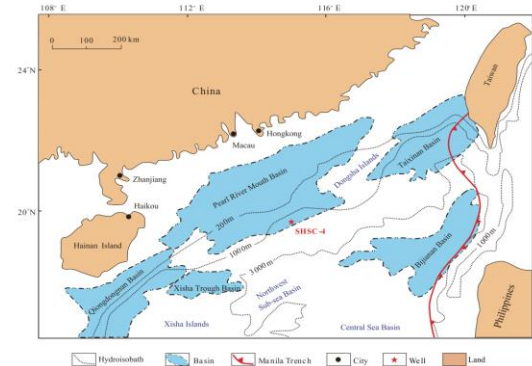


Fig. 1 The target area of the first NGH production test in Shenhu area, South China Sea<sup>[11]</sup>

### 2.2 Simulation model

The simulation software adopted TOUGH + HYDRATE (T+H) codes, developed by Lawrence Berkeley National Laboratory [20]. T+H codes included coupled flow-thermal-chemical modules that could model the non-isothermal gas release, phase changes, mass and heat transfer in porous media. The accuracy of simulation depended on the refinement of physical model and parameter of the modules' equations.

Fig. 2 shows the well design of production strategies in different layers in the hydrate deposit. A two-dimensional cylindrical model, with a radius of 78 m and a depth of 117 m, was established to describe the hydrate deposit of Shenhu area. This model consisted of HYDRA, HYDRB, MUDDY, overburden and underburden. This model was divided into 31×42=1302 grids, and the

# This is a paper for the 14<sup>th</sup> International Conference on Applied Energy - ICAE2022, Aug. 8-11, 2022, Bochum, Germany.

grids around the production well was subdivided to fit the analysis of the mass and heat transfer. The grids of the overburden, underburden and production well were set to be the inactive cells, of which reservoir properties were constant during the production processes. In this study, a vertical well completely penetrated the reservoirs was established and the depressurization method with constant pressure of 5.0 MPa was used for gas production from the hydrate deposit. The production strategies in different layers were following: (1) Case 1. Well A with a length of 35 m was arranged in the hydrate layer I (HYDRA); (2) Case 2. Well B with a length of 15 m was in the hydrate layer II (HYDRB); (3) Case 3. Well C with a length of 27 m was in the free gas layer (MUDDY).

The vertical well was located at the center of the cylinder model with a radius of 0.1 m. Assuming that the porosity of the production well was 1.0, and its permeability was following Darcy's law and set to 1000 D, and the capillary pressure is 0 Pa. The porosity, permeability and phase saturations of HYDRA, HYDRB, and MUDDY were consistent with the above introduction in geological background, respectively. The underlying layer (Overburden) was located below -1495 ~ -1475 m sea level, with pores filled with liquid water, and its porosity and permeability are the same as those of the hydrate layer I. The underlying layer (Underburden) was located at the lower part of the free gas layer, with a thickness of 20 m and -1572~-1545 m below the sea level, and its porosity and permeability are the same as those of the free gas layer (MUDDY). Hydrate layer I and hydrate layer II both belonged to the hydrate-bearing layers, and their temperature and pressure could satisfy the conditions for hydrate formation. Meanwhile, the temperature of the free gas layer is relatively high that hydrate did not keep stable. The initial pressure at the bottom of the HYDRB is 15.50 MPa, and the initial temperature is 16.59 °C. The pressure gradient and temperature gradient of the sediment are 0.01 MPa/m and 0.0443 °C/m, respectively. The main parameters and reservoir conditions of the simulation area are shown in Table 1.

Table 1 The main parameters and reservoir conditions of the simulation area

Parameter	value
Initial pressure of HYDRB	15.50 MPa
Initial temperature of HYDRB	16.59 °C
Initial porosities and phase saturations	Overburden ( $S_A = 1.00, \phi = 0.35$ ) HYDRA ( $S_H = 0.34, S_A = 0.66, \phi = 0.35$ )

	HYDRB ( $S_H = 0.31, S_A = 0.612, S_G = 0.078, \phi = 0.33$ ) Free gas layer ( $S_A = 0.922, S_G = 0.078, \phi = 0.32$ ) Underburden ( $S_A = 1.00, \phi = 0.32$ )
Gas component	100% CH <sub>4</sub>
Thermal gradient	0.0443 °C/m
Pore seawater salty	3.05%
	Overburden & HYDRA $2.9 \times 10^{-15} \text{ m}^2$ (2.9 mD)
Intrinsic permeability $k$	HYDRB $1.5 \times 10^{-15} \text{ m}^2$ (1.5 mD) MUDDY & Underburden $7.4 \times 10^{-15} \text{ m}^2$ (7.4 mD)
Well permeability	$1 \times 10^{-9} \text{ m}^2$ (1000 D)
Wet thermal conductivity $k_{ORW}$	1.7 W/m/K
Dry thermal conductivity $k_{ORD}$	1.0 W/m/K
Capillary pressure model [15, 16]	$P_{cap} = -P_0 [(S^*)^{-1/\lambda} - 1]^{1-\lambda}$ $S^* = (S_A - S_{irA}) / (S_{mA} - S_{irA})$
$S_{irA}$	0.30
$\lambda$	0.45
$P_0$	$10^5 \text{ Pa}$
Relative permeability model [16, 17]	$k_{rA} = (S_A^*)^n, k_{rG} = (S_G^*)^{nG}$ $S_A^* = (S_A - S_{irA}) / (1 - S_{irA})$ $S_G^* = (S_G - S_{irG}) / (1 - S_{irA})$
$n$	3.572
$n_G$	3.572
$S_{irG}$	0.030

### 3. RESULTS AND DISCUSSION

#### 3.1 Gas and water production

Fig. 3 shows the cumulative gas/water production of the production strategies in different layers for 10 years. In the early stage of production, the reservoir pressure around the well dropped quickly, resulting in the gas and water accumulated into the production well. For 10 years' continuous production, the cumulative gas production  $V_G$  of Case 1, Case 2 and Case 3 were  $1.73 \times 10^6$ ,  $1.18 \times 10^6$ , and  $3.86 \times 10^6 \text{ m}^3$ , respectively. The cumulative water production  $V_W$  of Case 1, Case 2 and Case 3 were  $1.92 \times 10^5$ ,  $0.46 \times 10^5$ , and  $5.94 \times 10^5 \text{ m}^3$ , respectively. Among the three production case of different layer, Case 3 had the largest cumulative gas production and cumulative water production. The cumulative gas production  $V_G$  and cumulative water production  $V_W$  of these three cases had the similar increasing trend during the production. The upward trend of  $V_G$  of those cases gradually slowed down in the later stage. It was due to the facts that the free gas stored in the reservoirs were consumed and the dissociated gas from hydrate was relatively small to supply the free gas resources. Fig. 4 shows the daily gas/water production of

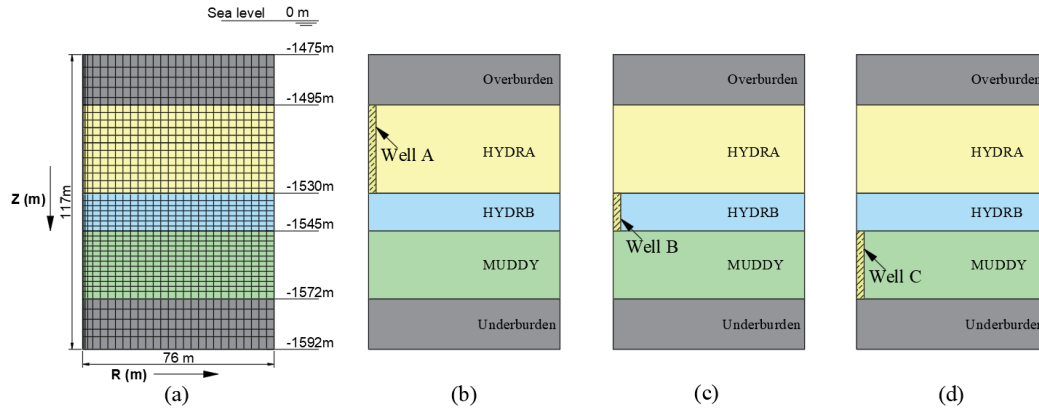


Fig. 2 The grid model and well design of production strategies in different layers in the hydrate deposit

the production strategies in different layers for 10 years. The daily gas production  $V_{dg}$  of Case 1-2 firstly gradually increased, and then kept relatively stable. As for the perspective of the production efficiency, the average daily gas production was closely related to the length of the vertical well. In 10 years' production, the daily gas production  $V_{dg}$  of Case 1 and Case 2 were 13.6 and 22.4 m<sup>3</sup>/day/m of well, respectively. At the same time, the corresponding daily water production  $V_{dw}$  of Case 1 and Case 2 gradually increased and reached to 1.5 and 0.8 m<sup>3</sup>/day/m of well, respectively. However, the daily gas production of Case 3 dropped quickly in the initial stage, and then gradually decreased during the production processes. The  $V_{dg}$  and  $V_{dw}$  of Case 3 were 1853.2 and 90.6 m<sup>3</sup>/day (68.6 and 6.1 m<sup>3</sup>/day/m of well) for 10 years, respectively. Among these three cases, the daily gas production and the daily water production of Case 3 in free gas layer was the highest, while Case 1 in hydrate layer I could obtain a more stable daily gas production in the long-term production processes. This indicated that the free gas layer production with relatively high permeability had a larger gas production potential than the other two cases.

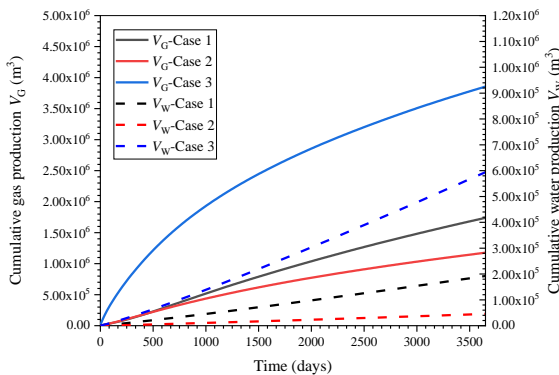


Fig. 3 Cumulative gas/water production of the production strategies in different layers for 10 years

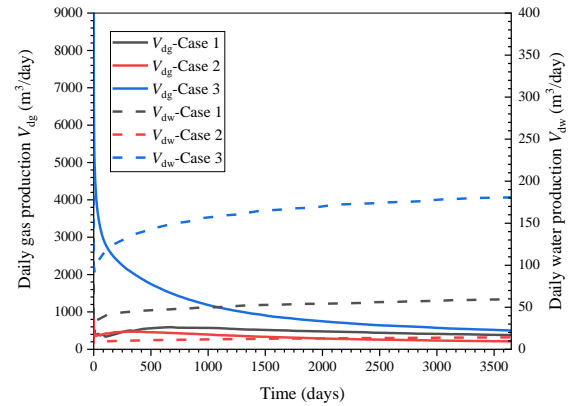


Fig. 4 Daily gas/water production of the production strategies in different layers for 10 years

Fig. 5 shows the gas-to-water ratio  $R_{GW}$  of the production strategies in different layers for 10 years. The  $R_{GW}$  referred to the ratio of the cumulative gas production to the cumulative water production ( $V_G/V_W$ ). The  $R_{GW}$  of Case 1 first decreased rapidly, and then increased to 13.6, final slowly decreased, of which values remained at 9.0-15.0 during the production processes. The  $R_{GW}$  of Case 2 appeared a rapid decline in the initial stage, stabilized at around 45.49 within 100-500 days, and then gradually decreased. After 10 years of continuous production, the  $R_{GW}$  of Case 1, Case 2 and Case 3 were 9.04, 25.80 and 6.48, respectively. Due to the hydrate deposit was far away from the sea level, it required a large amount of energy consumption for pumping the produced fluid to the offshore platform. After 1000 days' production, the  $R_{GW}$  of Case 1 and Case 3 is less than 20, and the water production is relatively large that had no economic value. Since the free gas layer had a higher permeability and water saturation, it would achieve a higher water production. In the long term production of 10 years, the production strategy of Case 1 would have a steady production potential with a relatively high  $R_{GW}$ .

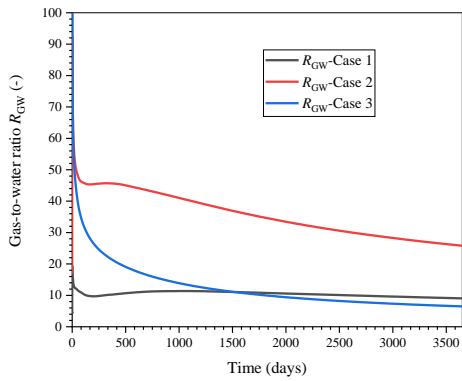


Fig. 5 Gas-to-water of the production strategies in different layers for 10 years

### 3.2 Evolution of the reservoir performances

Fig. 6 shows the evolution of spatial distribution of pressure of the hydrate reservoir over time. During the depressurization process, the pressure drop gradually spreads from the production well to the hydrate reservoir. Due to the pressure gradient of the reservoir, the depressurize rate had different performances in these cases. It was assumed that the area of pressure less than 13 MPa was the pressure-drop region. For 10 years production the area of Case 1 was mainly in range of about 80 m along the vertical well, and 30 m and 40 m were those of Case 2 and Case 3, respectively. The another important influencing factor was the intrinsic permeability of different layers. The low permeability layer of hydrate layer II could cause a relatively low depressurize rate, where the fluid flow of the reservoir was limited. Fig. 7 shows the evolution of spatial distribution of temperature of the hydrate reservoir over time. As shown in Fig. 7, within 60 days and 365 days of production, there would be a low temperature region appeared near the production well of Case 1 and Case 2. The low temperature area of Case 1 is more obvious due to the temperature gradient. When the reservoir pressure drops below the phase equilibrium pressure at the corresponding temperature, the hydrate dissociation reaction could be induced. The dissociation of hydrate would consume amounts of reservoir sensible heat, resulting the drop of the reservoir temperature. On the other hand, it was also a special performance for analyzing the hydrate dissociation area. In the late stage of 1825 and 3650 days, the changes of hydrate dissociation around the well gradually slowed down. The depressurization method had a limit for the pressure drop for long term production.

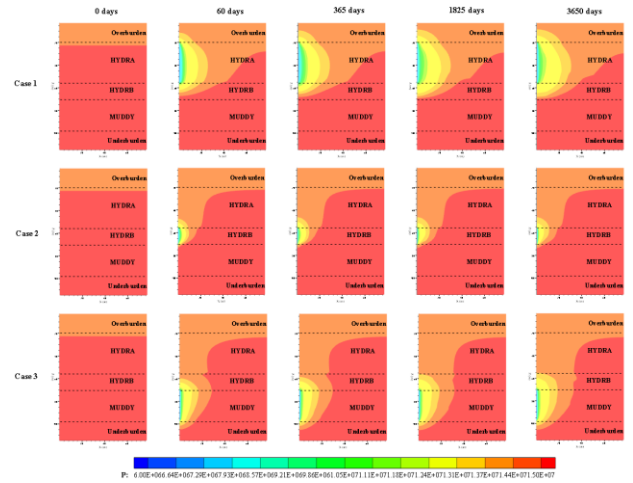


Fig. 6 Spatial distribution of pressure of hydrate reservoir over time

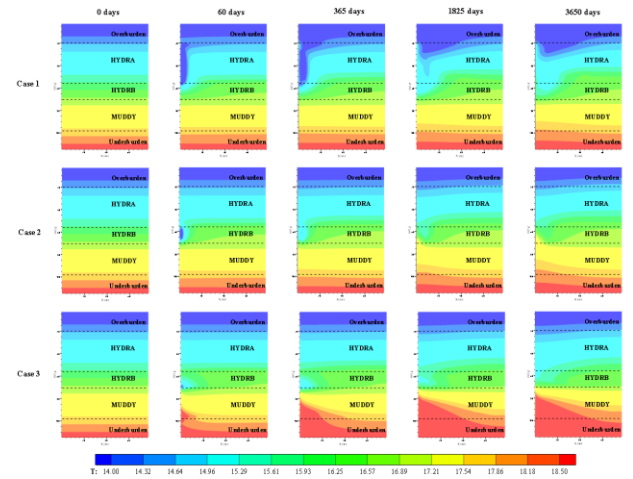


Fig. 7 Spatial distribution of temperature of hydrate reservoir over time

Fig. 8 shows the evolution of spatial distribution of hydrate saturation of the hydrate reservoir over time. During the depressurization process, due to the drop of reservoir pressure, the thermodynamic stability of the hydrate was broken, and the hydrate was dissociated to produce natural gas and water. The region of hydrate dissociation gradually expanded from the well to the surrounding reservoir. For 10 years' production, the hydrate dissociation region of Case 1 and Case 2 was spread to 20 m and 12 m, respectively. For the Case 3, there was no hydrate existed in the free gas layer, and hydrate in the hydrate layer II could be dissociated due to the water intrusion from free gas layer. The hydrate dissociation region of Case 3 is like a "skirt", and it expands to 30 m. With the strong driving force of depressurization, the water with relatively high temperature flowed into the wells that could promote the hydrate dissociation.

that could have appeared to influence the work reported in this paper.

## REFERENCE

- [1] Sloan ED, Koh CA. Clathrate hydrates of natural gases 2007.
- [2] Englezos P. Clathrate Hydrates. Ind Eng Chem Res 1993;32(7):1251-74.
- [3] Makogon YF. Natural gas hydrates – A promising source of energy. J Nat Gas Sci Eng 2010;2(1):49-59.
- [4] Hancock S, Collett T, Dallimore S. Overview of thermal-stimulation production-test results for the JAPEx/JNOC/GSC et al. Mallik 5L-38 gas hydrate production research well. Bulletin 585 ed. Northwest Territories, Canada: Geological Survey of Canada; 2005.
- [5] Numasawa M, Yamamoto K, Yasuda M, et al. Objectives and operation overview of the 2007 JOGMEC/NRCAN/Aurora Mallik 2L-38 gas hydrate production test. International Conference on Gas Hydrates: Dept. of Chemical Engineering; 2008. p. 1-10.
- [6] Boswell R, Schoderbek D, Collett TS, et al. The inik sikumi field experiment, alaska north slope: design, operations, and implications for co<sub>2</sub>-ch<sub>4</sub> exchange in gas hydrate reservoirs. Energ Fuel 2016;31(1):140-53.
- [7] Yamamoto K, Terao Y, Fujii T, et al. Operational overview of the first offshore production test of methane hydrates in the Eastern Nankai Trough. Offshore Technology Conference. Houston, Texas, USA 2014.
- [8] Yamamoto K, Wang XX, Tamaki M, et al. The second offshore production of methane hydrate in the Nankai Trough and gas production behavior from a heterogeneous methane hydrate reservoir. RSC Advances 2019;9(45):25987-6013.
- [9] Wu NY, Yang SX, Zhang HQ, et al. Gas hydrate system of shenhu area, northern south china sea: wire-line logging, geochemical results and preliminary resources estimates. Proceedings of the Annual Offshore Technology Conference 2010. p. 20485.
- [10] Wei W, Zhang JH, Wei XH, et al. Resource potential analysis of natural gas hydrate in South China Sea. Progress in Geophysics 2012;27(6):2646-55.
- [11] Li JF, Ye JL, Qin XW, et al. The first offshore natural gas hydrate production test in South China Sea. China Geology 2018;1(1):5-16.
- [12] Ye JL, Qin XW, Xie WW, et al. The second natural gas hydrate production test in the South China Sea. China Geology 2020;3(2):197-209.
- [13] Moridis GJ, Collett TS. Gas Production from Class 1 Hydrate Accumulations. New York 2004.
- [14] Zhang W, Liang JQ, Wei JG, et al. Origin of natural gases and associated gas hydrates in the Shenhu area, northern South China Sea: Results from the China gas

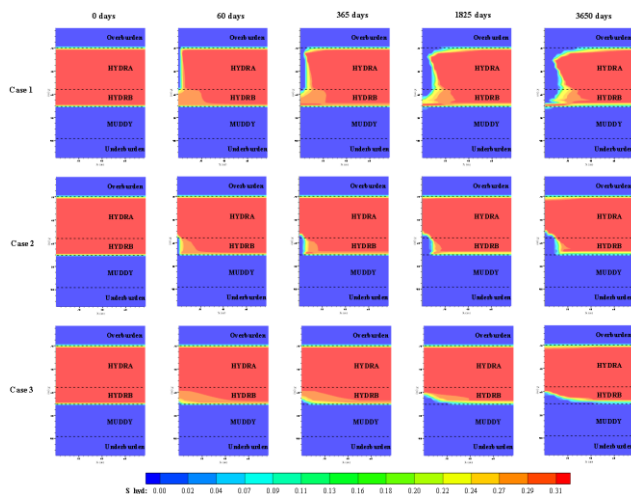


Fig. 8 Spatial distribution of hydrate saturation of the hydrate reservoir over time

## 4. CONCLUSIONS

(1) After 10 years of depressurization production, cumulative gas production of Case 1, Case 2 and Case 3 were  $1.73 \times 10^6$ ,  $1.18 \times 10^6$ , and  $3.86 \times 10^6$  m<sup>3</sup>, respectively. The cumulative water production  $V_w$  of Case 1, Case 2 and Case 3 were  $1.92 \times 10^5$ ,  $0.46 \times 10^5$ , and  $5.94 \times 10^5$  m<sup>3</sup>, respectively.

(2) The daily gas production of Case 3 gradually decreased during the production processes, while the daily water production continued to increase. However, Case 1 and Case 2 could obtain a more stable daily gas production for long-term production.

(3) The gas-to-water ratio of Case 2 was larger than the other two production cases, indicating that in terms of production energy consumption, the production strategy of well design in hydrate layer II could effectively improve gas production efficiency.

(4) The intrusion of the relatively high-temperature water could improve the hydrate dissociation at the bottom of the hydrate layer.

## ACKNOWLEDGEMENT

The authors are very grateful for the support of the National Natural Science Foundation of China (51976228), Key Program of National Natural Science Foundation of China (51736009), the Special Project for Marine Economy Development of Guangdong Province (GDME-2020D044), and the Frontier Sciences Key Research Program of the Chinese Academy of Sciences (QYZDB-SSWJSC028; QYZDJ-SSW-JSC033), which are gratefully acknowledged.

## DECLARATION OF INTEREST STATEMENT

The authors declare that they have no known competing financial interests or personal relationships

hydrate drilling expeditions. *Journal of Asian Earth Sciences* 2019;183:103953.

[15] Van Genuchten MT. A closed-form equation for predicting the hydraulic conductivity of unsaturated soils *Soil Sci Soc Am J* 1980;44(05):892-8.

[16] Stone HL. Probability Model for Estimating Three-Phase Relative Permeability. *J Pet Te* 1970;22(02):214-8.

[17] Moridis GJ, Kowalsky M, B, Pruess K. TOUGH+Hydrate v1.0 User's Manual: A Code for the Simulation of System Behavior in Hydrate-Bearing Geologic Media. Earth Sciences Division. Lawrence Berkeley National Laboratory, Berkeley, 2008.